

# Ion yield improvement for static secondary ion mass spectrometry by use of polyatomic primary ions

Roel De Mondt<sup>1\*</sup>, Luc Van Vaeck<sup>1</sup>, Andreas Heile<sup>2</sup>, Heinrich F. Arlinghaus<sup>2</sup>, Nicolas Nieuwjaer<sup>3</sup>, Arnaud Delcorte<sup>3</sup>, Patrick Bertrand<sup>3</sup>, Jens Lenaerts<sup>4</sup> and Frank Vangaveer<sup>4</sup>

<sup>1</sup>MiTAC, University of Antwerp, Department of Chemistry (CDE), Universiteitsplein 1, B-2610 Wilrijk, Belgium

<sup>2</sup>Westfälische Wilhelms-Universität Münster, Physikalisches Institut, Wilhelm-Klemm-Str. 10, 48149 Münster, Germany

<sup>3</sup>Université Catholique de Louvain (UCL), Unité Physico-Chimie et Physique des Matériaux (PCPM), Croix du Sud 1, B-1348 Louvain-la-Neuve, Belgium

<sup>4</sup>Agfa Graphics N.V., Septestraat 27, B-2640 Mortsel, Belgium

Received 6 November 2007; Revised 6 March 2008; Accepted 10 March 2008

Static secondary ion mass spectrometry (S-SIMS) is one of the potentially most powerful and versatile tools for the analysis of surface components at the monolayer level. Current improvements in detection limit (LOD) and molecular specificity rely on the optimisation of the desorption-ionisation (DI) process. As an alternative to monoatomic projectiles, polyatomic primary ion (P.I.) bombardment increases ion yields non-linearly. Common P.I. sources are Ga<sup>+</sup> (liquid metal ion gun (LMIG)), SF<sub>5</sub><sup>+</sup> (electron ionisation) and the newer Au<sub>n</sub><sup>+</sup>, Bi<sub>n</sub><sup>q+</sup> (both LMIG) and C<sub>60</sub><sup>+</sup> (electron ionisation) sources. In this study the ion yield improvement obtained by using the newly developed ion sources is assessed. Two dyes (zwitterionic and/or thermolabile polar functionalities on a largely conjugated backbone) were analysed as a thin layer using Ga<sup>+</sup>, SF<sub>5</sub><sup>+</sup>, C<sub>60</sub><sup>+</sup>, Bi<sup>+</sup>, Bi<sub>3</sub><sup>2+</sup> and Bi<sub>5</sub><sup>2+</sup> projectiles under static conditions. The study aims at evaluating the improvement in LOD, useful and characteristic yield and molecular specificity. The corrected total ion count values for the different P.I. sources are compared for different instruments to obtain a rough estimate of the improvements. Furthermore, tentative ionisation and fragmentation schemes are provided to describe the generation of radical and adduct ions. Characteristic ion yields are discussed for the different P.I. sources. An overview of the general appearances of the mass spectra obtained with the different P.I. sources is given to stress the major improvement provided by polyatomic P.I.s in yielding information at higher *m/z* values. Copyright © 2008 John Wiley & Sons, Ltd.

The analytical chemist faces a growing demand for methods capable of probing the molecular composition of ingredients and sometimes their (unknown) interaction products with a depth resolution of only one monolayer and, preferentially, a lateral resolution in the sub  $\mu\text{m}$ -range. Molecular specificity is of the utmost importance in dealing with the locally complex mixtures of 'as received' solids. Static secondary ion mass spectrometry (S-SIMS) is widely recognised as one of the most useful analytical methods of dealing with the selective chemical characterisation of a wide range of organic and inorganic surface components at the monolayer level. With the advent of time-of-flight (TOF) S-SIMS and the availability of adequate fast electronics, the limits of instrumental improvements seem to have been reached and further progress with respect to limit of detection (LOD) and molecular specificity is now being pursued by the

development of new approaches, involving fundamental optimisation of the desorption-ionisation (DI) process. Deposition of a thin layer of gold on the sample has been shown to improve ion yields dramatically in a variety of cases, but this involves the risk of modifying the composition of the pristine surface.<sup>1,2</sup> Polyatomic primary ion (P.I.) bombardment, as an alternative to the traditionally used monoatomic projectiles, has been shown to allow ion yields to be increased non-linearly.<sup>3–5</sup> Initial reports using beams with relatively large spots have evidenced a large potential for organic analysis.<sup>6</sup> In recent years several groups have developed different types of P.I. guns allowing the advantage of increased ion yield to be combined with the potential of high lateral resolution analysis. Specifically, a converted electron ionisation (EI) source has been used for SF<sub>5</sub><sup>+</sup> P.I. beams with a spot size of 20  $\mu\text{m}$ .<sup>7</sup> The liquid metal ion gun (LMIG) technology has been adapted to produce Au<sub>n</sub><sup>+</sup> and more recently Bi<sub>n</sub><sup>+</sup> cluster beams.<sup>8</sup> An alternative approach used EI on heated C<sub>60</sub> to obtain a C<sub>60</sub><sup>+</sup> projectile beam with a spot size of a few  $\mu\text{m}$  on the sample.<sup>9,10</sup>

Unfortunately, the discussed publications focusing on the development of the new ion guns tend to include tests on

\*Correspondence to: R. De Mondt, MiTAC, University of Antwerp, Department of Chemistry (CDE), Universiteitsplein 1, B-2610 Wilrijk, Belgium.

E-mail: roel.demondt@ua.ac.be

Contract/grant sponsor: IWT-Flanders, FWO Flanders and EC NoE Nanobeams.

different samples, thus preventing the direct comparison of the specifications and performances in practical material analysis. The purpose of this study is to introduce a systematic comparison of different P.I. guns on the same sample. We describe herein a comparison of the results for two selected polyfunctional dyes that have been analysed with  $\text{Ga}^+$ ,  $\text{SF}_5^+$ ,  $\text{C}_{60}^+$ ,  $\text{Bi}^+$  and  $\text{Bi}_n^{q+}$  P.I. sources under static conditions. The experiments aim at evaluating, for each gun relative to the others, the improvement in LOD, useful and characteristic yield and molecular specificity. In these preliminary experiments, determination of 'absolute LOD' on verified monolayers is not yet aimed at. Therefore, sample preparation as thin layers via spin coating on Si wafers has been considered to be appropriate as it allows (under the conditions used here) laterally homogeneous layers with reproducible thickness to be obtained. Future work must include thick molecular films, or thin films on molecular substrates, on which cluster ion bombardment is reported to be highly beneficial.<sup>6,11–14</sup>

The studied compounds are directly relevant to practical applications in advanced research and material developments in the field of digital imaging. However, the samples can be considered as a good starting point for a variety of applications where low molecular weight (MW) compounds are to be analysed. The actual selection of the test compounds was motivated by their chemical structures in terms of zwitterionic and thermolabile polar functionalities on a largely conjugated backbone structure. As a result, the structures lend themselves to the generation of radical ions, which are highly relevant in revealing information about the different projectile bombardment conditions used. Modelling studies systematically point to increased energy deposition in a region closer to the surface.<sup>15</sup> However, the further linking to the detected ions remains limited by the calculation capability and the inability to include a good model for ion formation.<sup>16</sup> Analytical chemists can, of course, use their knowledge of MS and the information gathered from experimental databases to get insight in the parameters that are of importance to the optimal generation of structurally significant ions. A consistent and detailed structural assignment of the detected ions significantly increases specificity in the analysis of unknown samples. From theoretical and practical studies on the sputtering with polyatomic sputtering ions in SIMS, it seems that the mass, size, energy and number of atoms within the projectile are all important in the observed non-linear increase of the ion yield.<sup>3,4,17–19</sup> In this respect, the P.I. guns used in this study provide a range of conditions. Specifically,  $\text{Ga}^+$  bombardment with a LMIG can be considered as the reference. The  $\text{SF}_5^+$  projectiles have a relatively high number of impacting atoms with a relatively small cluster mass ( $m/z$  127). The results have already been compared with those from  $\text{Xe}^+$  and  $\text{Ga}^+$  bombardment to verify that the ion yield increase comes in part from mass and in part from the number of atoms. Use of  $\text{Bi}^+$  gives a projectile with a high mass ( $m/z$  209) and application of  $\text{C}_{60}^+$  represents the ultimate in size, mass and number of atoms. The projectiles  $\text{Bi}_3^{2+}$  and  $\text{Bi}_5^{2+}$  are a special case in that they are not only heavier than the traditional monoatomic P.I.s, but also doubly charged.

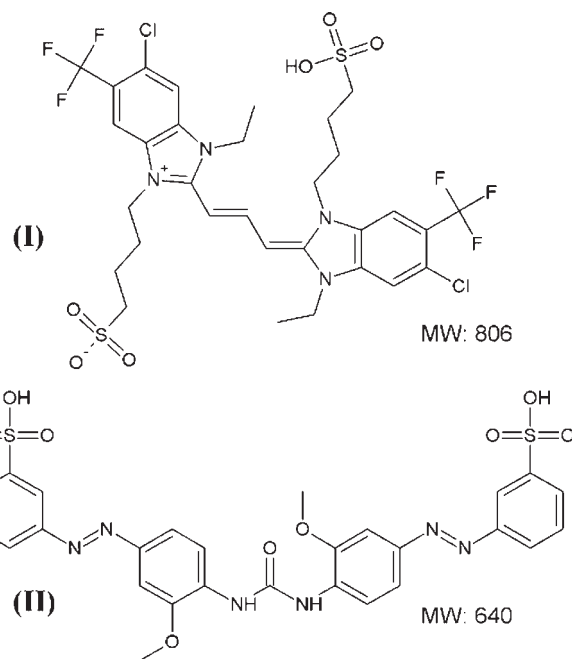


**Figure 1.** Structures of the studied compounds, notation I and II as indicated.

## EXPERIMENTAL

### Samples

Chemicals were provided by Agfa-Gevaert (Mortsel, Belgium). The molecular structures are shown in Fig. 1. Samples were prepared by spin coating 10  $\mu\text{L}$  of a 1 mg  $\text{mL}^{-1}$  solution of compound I in 2-butanone (99+%, Acros, Geel, Belgium) and 20  $\mu\text{L}$  of a 0.1 mg  $\text{mL}^{-1}$  solution of compound II in  $\text{H}_2\text{O}$  on Si at 2000 rpm. The silicon wafers were test grade silicon (14.5–20 Ohm cm, Montco Silicon, Spring City, PA, USA). They were thoroughly cleaned by 10 min of sonification in methanol and dried in a stream of hot air. Spin coating was performed with a Cookson electronic equipment SCS G3-8 (PI-KEM Ltd, Tamworth, UK) at 2000 rpm, with an acceleration time of 20 s, spin time of 35 s and a deceleration time of 10 s.

### Instrumental

The TOF-SIMS experiments were carried out on three different instruments: a TRIFT 1 TFS-4000MMI (PHI-EVANS, Sunnyvale, CA, USA)<sup>20</sup> equipped with a  $\text{Ga}^+$  and an IOG-C60-20  $\text{C}_{60}^+$  P.I. source (Ionoptika Ltd., Chandler's Ford, UK)<sup>21</sup> (PCPM) and two TOF-SIMS IV instruments (Ion TOF, Münster, Germany) equipped with a  $\text{Bi}_n^{q+}$  and an  $\text{SF}_5^+$  P.I. source (Münster group) and a  $\text{Ga}^+$  and  $\text{SF}_5^+$  P.I. source, respectively (MiTAC). The experimental conditions of the different analyses are shown in Table 1. The best comparisons of ion yields should be achieved by operating all the guns at the same P.I. energy. However, previous round robin experiments have shown us that use of the best settings (defined by the operator's experience and the precise construction or version of the instrument) is beneficial for the analytical use of the data in terms of sensitivity and precision. It is well known that the P.I. energy influences the ion yield through a more or less linear relationship but

**Table 1.** Experimental conditions of different P.I. sources. For samples of compounds I and II the same settings were used with the same P.I. source

	Ga <sup>+</sup>	SF <sub>5</sub> <sup>+</sup>	Bi <sup>+</sup>	Bi <sub>3</sub> <sup>2+</sup>	Bi <sub>5</sub> <sup>2+</sup>	C <sub>60</sub> <sup>+</sup>
Current (pA)	0.2	0.06	0.2	0.03	0.03	0.02–0.03
Analysis time (s)	150	200	200	200	200	180
Area (μm <sup>2</sup> )	100 × 100	100 × 100	100 × 100	100 × 100	100 × 100	130 × 130
Energy (keV)	25	10	25	25	25	+ 12    - 18
Primary ion dose density (# P.I. cm <sup>-2</sup> )	1.88 × 10 <sup>12</sup>	7.5 × 10 <sup>11</sup>	2.5 × 10 <sup>12</sup>	1.88 × 10 <sup>11</sup>	1.88 × 10 <sup>11</sup>	2.31–3.46 × 10 <sup>11</sup>

LMIGs have operating voltages that are inherently much higher than are feasible with EI sources.

Every sample has been analysed twice in positive ion as well as negative ion detection mode to verify the reproducibility (typically better than 10% relative standard deviation (RSD)). The ion dose has been kept below 10<sup>13</sup> ions cm<sup>-2</sup> and therefore the analyses are considered to be performed in the so-called static regime. The static regime in SIMS can be explained as follows. As the impact of a P.I. destroys the molecular structures in the sample over a given area (typically 10 nm<sup>2</sup>) around the point of impact, detection of molecular information implies that no spot should be hit twice. The static limit refers to the maximum allowable ion dose density that makes less than 1% of the surface area inadequate for further analysis. A full discussion is given elsewhere.<sup>22</sup>

## RESULTS AND DISCUSSION

The systematic evaluation of the data will be organised as follows. First, instrument-related features such as mass resolution and mass accuracy will be discussed, as these are essential to exploit the information contained in the mass spectra. Subsequently, improved detection capabilities due to the different types of polyatomic P.I.s are characterised by means of the total ion production, measured by the total ion count (TIC) parameter or per given dose of projectiles.

Following the same reasoning, the subsequent discussion treats the relative ion yields for selected ions per given dose of P.I.s. Further evaluation of the mass spectra addresses the detection of additional or different ions depending on the projectile used and the relative contribution of structurally significant analyte ions in comparison with the low *m/z* ions such as C<sup>+</sup>, CH<sub>3</sub><sup>+</sup>, C<sub>2</sub>H<sub>3</sub><sup>+</sup>... with relatively low diagnostic value. The relative contributions of different ions from a given molecule can be useful in distinguishing different energy regimes induced on the sample by the different P.I. sources. The *m/z* values of the ions mentioned throughout this manuscript refer to the structure with the most abundant isotopes (e.g. <sup>35</sup>Cl).

### Mass resolution and mass accuracy

The mass resolution was calculated on the H<sup>+/-</sup> signal in the spectra generated with the different P.I. sources. The results are presented in Table 2(A). It is clear that both electron ionisation P.I. sources (SF<sub>5</sub><sup>+</sup> and C<sub>60</sub><sup>+</sup>) yield lower mass resolution. This is inherent to the ionisation mechanism used for P.I. generation and for C<sub>60</sub><sup>+</sup> the resolution was further reduced by the presence of C isotopes in the P.I. gun: a range of C<sub>60</sub><sup>+</sup> ions is emitted with masses *M*, *M*+1, *M*+2, causing bad time-focusing.

The Bi<sub>*n*</sub><sup>2+</sup> cluster sources are found to be better than the EI sources and the monoatomic P.I. sources appear to have the best mass resolution.

**Table 2.** Mass resolution of H<sup>+/-</sup> signal (A) and mass accuracies (B) of selected ions from compounds I and II upon analysis of I and II with the different P.I. sources in positive and negative polarity

		Ga <sup>+</sup>		SF <sub>5</sub> <sup>+</sup>		Bi <sup>+</sup>		Bi <sub>3</sub> <sup>2+</sup>		Bi <sub>5</sub> <sup>2+</sup>		C <sub>60</sub> <sup>+</sup>	
		+	-	+	-	+	-	+	-	+	-	+	-
<b>A: Mass resolution of H<sup>+/-</sup></b>													
I		2200	1700	1100	800	2400	2400	1700	1200	1500	1000	100	220
II		2000	1700	1100	800	2500	2200	1700	1300	1600	1000	110	140
I +	I -	<b>B: Mass accuracies of ions at given <i>m/z</i> (ppm)</b>											
233	219	34	242	77	74	33	21	69	44	73	56	210	0
248	355	32	n/a	55	76	16	29	46	25	46	24	246	85
275	383	33	n/a	53	69	18	28	38	27	37	27	105	80
385	397	31	n/a	26	60	4	18	18	14	10	10	323	79
807	399	n/a	n/a	37	166	23	128	9	114	33	110	314	18
II +	II -												
72	156	17	103	22	4	14	103	24	15	6	4	146	301
165	262	6	n/a	10	67	20	27	7	89	19	82	236	557
202	290	30	n/a	6	23	38	77	15	38	42	24	116	417
350	304	n/a	n/a	55	50	31	49	40	70	19	53	120	n/a
378	332	n/a	n/a	5	12	19	89	33	25	67	5	296	636

**Table 3.** Corrected useful total ion yield data for compounds I and II analysed with the different P.I. guns. The numbers refer to the number of secondary ions per given number of P.I. projectiles, corrected for instrumental variations. The numbers in parentheses refer to the useful total ion yield gain factors: these values are calculated by normalising to the value obtained using Ga<sup>+</sup> P.I.s

	I +	I -	II +	II -
C <sub>60</sub> <sup>+</sup>	0.71 (34)	0.060 (12)	0.15 (24)	0.027 (10)
Bi <sub>5</sub> <sup>2+</sup>	0.45 (21)	0.024 (5)	0.21 (33)	0.023 (9)
Bi <sub>3</sub> <sup>2+</sup>	0.46 (22)	0.026 (5)	0.11 (18)	0.019 (7)
Bi <sup>+</sup>	0.039 (2)	0.0023 (0.5)	0.010 (2)	0.0017 (0.6)
SF <sub>5</sub> <sup>+</sup>	0.14 (7)	0.0081 (2)	0.030 (5)	0.0059 (2)
Ga <sup>+</sup>	0.021(1)	0.0049 (1)	0.0063 (1)	0.0027 (1)

The data for mass accuracy of the analysis are given for a few diagnostic ions in Table 2(B). The differences in mass accuracy are rather small, except for C<sub>60</sub><sup>+</sup> P.I. bombardment. The ppm error values obtained from mass spectra with this P.I. source are remarkably high.

### Survey of total ion count (TIC) and relative ion yield data

The first question to be addressed concerns the total improvement in secondary ion production to be expected when the commonly used monoatomic Ga<sup>+</sup> projectiles are replaced by a polyatomic P.I. source. Table 3 surveys the useful total ion yield data for compounds I and II analysed with the different ion guns. The useful total ion yield refers to the number of secondary ions detected from a given number of projectiles impinging on the sample. In this case it corrects the actual TIC values for the individual P.I. intensity and for the pulse length of the different guns. Although useful total ion yield calculations account for these instrument-related differences, the transmission of the analyser and the efficiency of the detector also directly influence the result. These parameters can have dramatic effects on the useful total ion yield numbers as found when the Ga<sup>+</sup> or SF<sub>5</sub><sup>+</sup> data are compared for the two instruments, possibly because of the differences in mass analyser (reflectron vs. reflectron TOF and 3 90°-electrostatic sector mass spectrometer) and ion source construction. In order to fully estimate the useful total ion yield data, total normalisation was obtained by always using an ion source of the same kind when comparing instruments: Ga<sup>+</sup> in PCPM and MiTAC and SF<sub>5</sub><sup>+</sup> in the Münster and MiTAC group (cf. Instrumental section). In this way, a normalisation relative to the common sources was possible and the capabilities of all the sources could be estimated appropriately. Correction factors were calculated in such a way that the results obtained with Ga<sup>+</sup> and SF<sub>5</sub><sup>+</sup> on the respective two machines were identical. It is clear from Table 3 that C<sub>60</sub><sup>+</sup> and the Bi<sub>3</sub><sup>2+</sup> and Bi<sub>5</sub><sup>2+</sup> P.I. sources perform better in useful total ion yield than SF<sub>5</sub><sup>+</sup> cluster projectiles in all cases. The monoatomic Ga<sup>+</sup> and Bi<sup>+</sup> sources exhibit consistently lower useful total ion yields than the cluster projectiles.

The useful total ion yield data concern the sum of all detected ions. To evaluate the improvement in the analytical potential, the figures must be linked to the way in which this

TIC is distributed over the different ions. For instance, in the case of II measured with Ga<sup>+</sup>, the Na<sup>+</sup> signal accounts for 80% of the TIC while it is only 5–10% in all other cases. Also, for compound I the signal due to the accompanying pyrimido-azepine derivative contributes significantly to the TIC in cluster P.I. analysis as opposed to the other experiments. Whenever comparison of the gain in useful total ion yield, relative to Ga<sup>+</sup> results, without the contribution of the Na<sup>+</sup> with low diagnostic value is preferred, the indicative yield gain factors must be multiplied by 3. Even more important is taking specific ion yield into account. In Fig. 2 the ion intensities of a selection of relevant ions for compounds I and II are shown, normalised to the P.I. doses and corrected for instrumental parameters (cf. in case of TIC). However, the difference in projectile energy, which is known to influence the ion yield, is not explicitly accounted for. Not all sources can be operated at the same (high or low) beam energies. Therefore, correcting the data in Fig. 2 would give data that could not (yet) be obtained in practice.

The calculation of the correction factors in the case of the TIC was relatively straightforward, since the TIC can always be measured. In the case where specific ions are concerned, taking into account the relatively poor high *m/z* ion generation with Ga<sup>+</sup> bombardment, it gets more difficult. Figure 2(A) shows the corrected relative ion yield for positive ions from I. This is the best sample and mode for this comparison since all considered high *m/z* ions are detected with all guns. It is clear that Ga<sup>+</sup>, Bi<sup>+</sup> and SF<sub>5</sub><sup>+</sup> yield low relative secondary ion yields with the first one being worst and the last one being the best of these three. Furthermore, C<sub>60</sub><sup>+</sup> and Bi<sub>n</sub><sup>2+</sup> perform much better, with Bi<sub>3</sub><sup>2+</sup> yielding a slightly smaller number of ions per given number of projectiles. Comparison of these trends with the results in Fig. 2(B), where negative ions from compound I are graphed, is rather difficult. The Ga<sup>+</sup> ion source did not yield ions at *m/z* 355, 383, 397 or 399, which makes any further comparison with C<sub>60</sub><sup>+</sup> impossible if all instrumental parameters have to be taken into account. The ion at *m/z* 219 is the only one detected with all P.I. sources. Comparison of the corrected characteristic yields for *m/z* 219 shows the best performance for Bi<sub>n</sub><sup>2+</sup> (with a slightly higher yield for Bi<sub>3</sub><sup>2+</sup>), closely followed by C<sub>60</sub><sup>+</sup>. These recently developed polyatomic sources show more or less identical results, where the older SF<sub>5</sub><sup>+</sup> clusters give clearly lower yields. Monoatomic Ga<sup>+</sup> and Bi<sup>+</sup>, however, give very poor yields. Although the other high *m/z* ions are clearly present in the mass spectra obtained from C<sub>60</sub><sup>+</sup> bombardment, these results are perforce excluded from the following discussion due to the lack of Ga<sup>+</sup> data for calculation of the correction factor. For these higher *m/z* ions again the Bi<sub>n</sub><sup>2+</sup> clusters perform best in comparison with SF<sub>5</sub><sup>+</sup>, and Bi<sub>3</sub><sup>2+</sup>, Bi<sub>5</sub><sup>2+</sup> and SF<sub>5</sub><sup>+</sup> all outperform the Bi<sup>+</sup> projectiles. The results for II are given for positive ions in Fig. 2(C). It can be seen that again Ga<sup>+</sup> bombardment does not yield all high *m/z* ions, narrowing down the comparison with Bi<sub>n</sub><sup>q+</sup> projectiles and SF<sub>5</sub><sup>+</sup>. The results are in agreement with those obtained from compound I with these P.I. sources, with a slightly better result for Bi<sub>5</sub><sup>2+</sup>, although the best improvement is found in the less structurally significant cluster ion at *m/z* 72 (the results at *m/z* 72 for Bi<sub>3</sub><sup>2+</sup> were

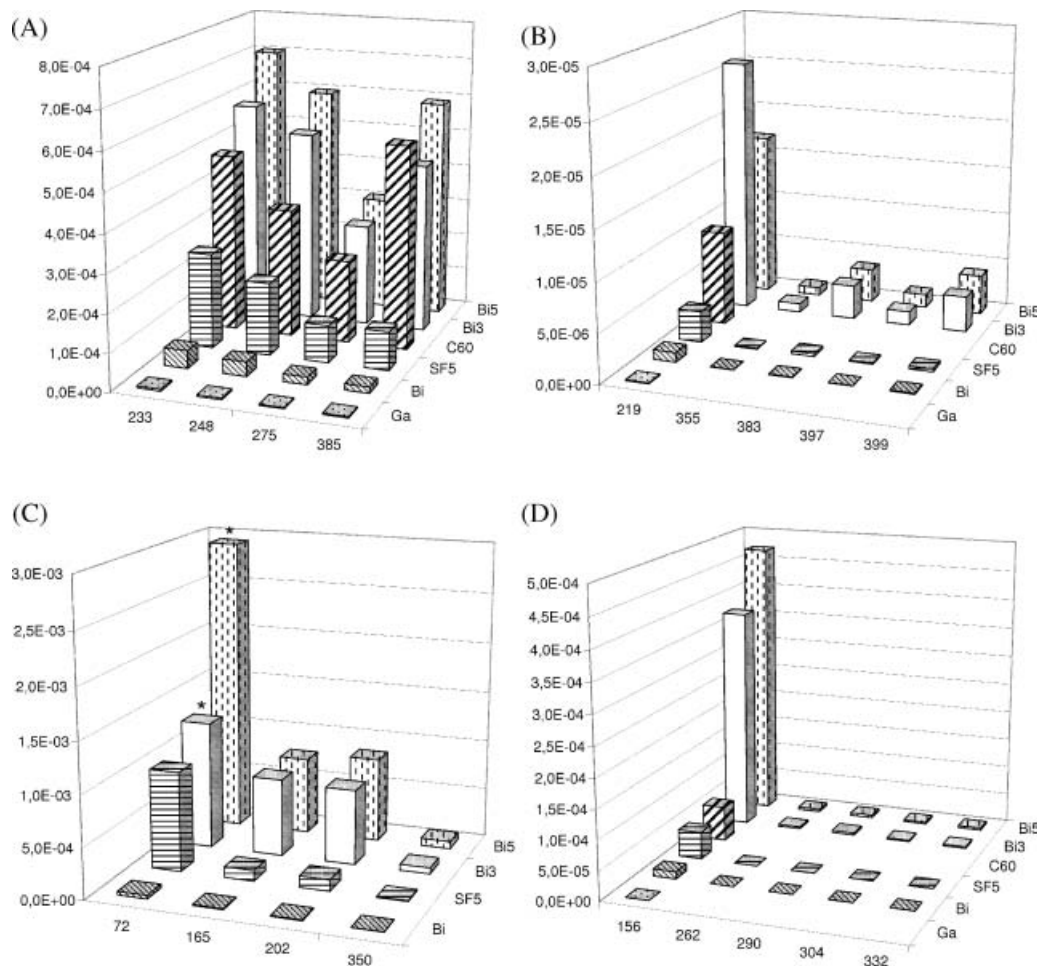


**Figure 2.** Corrected characteristic ion yields of positive (A) and negative (B) ions from I and positive (C) and negative (D) ions from II. The values indicated with an asterisk in (C) for  $m/z$  72 obtained with Bi<sub>3</sub><sup>2+</sup> and Bi<sub>5</sub><sup>2+</sup> are divided by 10 to enhance the graphical overview.

divided by 10 for graphical reasons). Figure 2(D) shows the results for negative ions of II and although it would be expected that the limitation of the C<sub>60</sub><sup>+</sup> results is again dictated by the performance of the Ga<sup>+</sup> source, in this case a remarkable result is found for C<sub>60</sub><sup>+</sup>: it appears not to be able to yield in a significant amount the ions at  $m/z$  262, 290, 304 and 332 and most of the desorption and ionisation phenomena seem to have resulted in the side-chain ion at  $m/z$  156. All other observations in the previously discussed Figs. 2(A), 2(B) and 2(C) still hold.

The necessary combination of useful total ion yield values and ion-specific characteristic ion yield reveals that the use of the Bi<sub>3</sub> or Bi<sub>5</sub> clusters does not make much difference and it is appropriate to state that in general Bi<sub>n</sub><sup>2+</sup> P.I.s cause a dramatic improvement in useful total ion yield, combined with major improvements in characteristic ion yield. The other newly developed cluster source, namely C<sub>60</sub><sup>+</sup>, also shows a great improvement in useful total ion yield, but the characteristic ion yield improvements are (as far as measurable) apparently more dependent on ion polarity and molecular structure, especially for the negative ions of II, where preferential formation of a side-chain ion was encountered. The SF<sub>5</sub><sup>+</sup> source gives useful total ion yield results that are better than those of monoatomic P.I.s, but does not establish the same improvement per P.I. as the recently developed cluster

sources. When comparing the monoatomic Ga and Bi, it is not fully shown that Bi yields higher TIC values, but a clear, yet moderate enhancement can be found for the characteristic ion yield. The main difference lies in whether or not an ion is detected using a given P.I. beam. Use of Bi<sup>+</sup> yields ions that cannot be detected when using Ga<sup>+</sup>. The ambiguity in the results on the TIC might be an effect of the low performance of one of the SF<sub>5</sub><sup>+</sup> sources which influences the correction factor and, as a consequence, the Bi<sub>n</sub><sup>q+</sup> results.

### Qualitative comparison of the mass spectra

Figure 3 compares the positive ion mass spectra from compound I with Ga<sup>+</sup>, Bi<sup>+</sup>, Bi<sub>5</sub><sup>2+</sup> and C<sub>60</sub><sup>+</sup> projectiles. The mass spectrum with the small monoatomic projectile Ga<sup>+</sup> exhibits the typical pattern with dominating signals primarily clustered around the typical hydrocarbon fragment ions at low  $m/z$  values up to  $m/z$  150. The heavier monoatomic Bi<sup>+</sup> causes substantial increase in the relative contribution from the high  $m/z$  diagnostic ions to the TIC. Actually, the base peak in the mass spectrum comes now from the pyrimido-azepine while the most intense signal from the zwitterionic structure itself is found at  $m/z$  385 which is a fragment ion keeping a substantial part of the original skeleton. Application of the polyatomic C<sub>60</sub><sup>+</sup> or doubly charged Bi<sub>5</sub><sup>2+</sup> projectiles further increases the relative

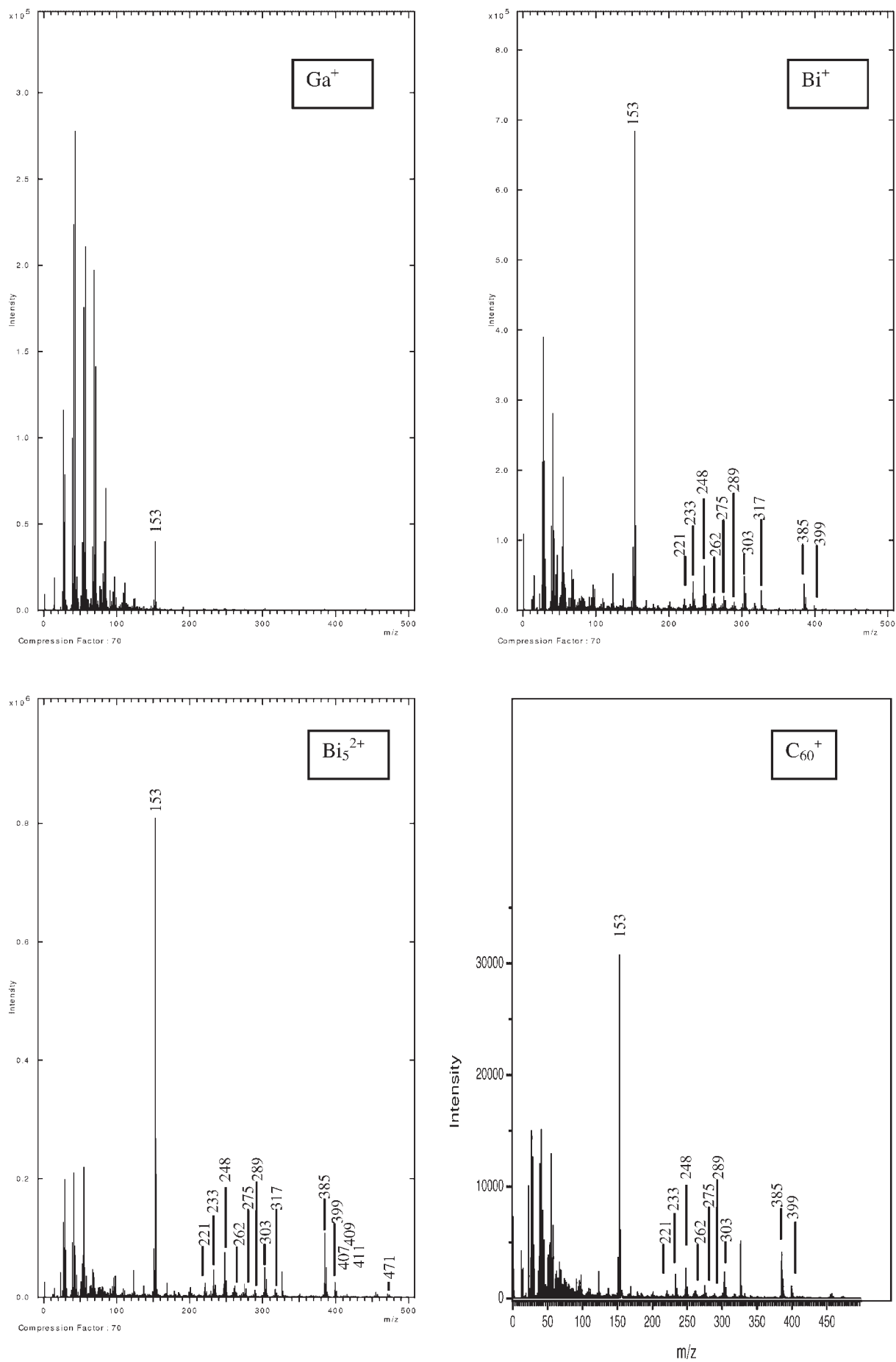


**Figure 3.** Positive ion mass spectra obtained from I using Ga<sup>+</sup>, Bi<sup>+</sup>, Bi<sub>5</sub><sup>2+</sup> and C<sub>60</sub><sup>+</sup> P.I.s.

importance of the high  $m/z$  ions while that of the ions  $< m/z$  100 reduces. Also, the predominance of the signal at  $m/z$  153 in comparison with the high mass fragment ions, at e.g.  $m/z$  385, is decreased. The mass spectrum taken with the  $\text{Bi}_3^{2+}$  projectiles closely resembles that shown for  $\text{Bi}_5^{2+}$  or  $\text{C}_{60}^+$ . The relative ion intensities seen with  $\text{SF}_5^+$  are reminiscent of those shown for  $\text{Bi}_3^{2+}$ .

It is important to combine these observations with the importance of specific ions with respect to diagnostic characterisation of the analyte. Table 4 lists the accurate mass measurements of diagnostic ions and Scheme 1 summarises the structural assignment and tentative fragmentation routes. The scheme has been composed using the basis principles of the empiric DI model, originally developed for laser microprobe mass spectrometry and later on found to be applicable to mass spectra in S-SIMS and other methods.<sup>23–25</sup> The DI model does not give a fundamental and detailed description of all aspects in the complex sputtering and ion formation process but provides a simple framework allowing us to rationalise the formation of the detected ions and their structural assignment. The used DI model differs from the earlier approach of Cooks and Busch<sup>26,27</sup> by introducing the effects of energy, time and local pressure as key parameters to explain the observed ions. The DI model assumes the initial release of organic molecules and salts as neutrals or ion pairs, respectively. The local conditions allow that even thermolabile can be set free without decomposition. However, the thermal decomposition route also remains active. The released neutrals in the seldedge (gas-phase zone with high collision probability just above the sample) become ionised either by EI producing  $\text{M}^{+\bullet}$  or  $\text{M}^{\bullet-}$  with high internal stress or by adduct ionisation (AI), yielding adduct ions with low internal energy. The fragmentation occurs according to the common routes known from gas-phase mass spectrometry, taking into account that the amount of internal stress can be different from that of analytes ionised in conventional EI or chemical ionisation sources. In practice, the majority of the daughter

ions are assumed to originate from radical ions and that is why the corresponding molecular ion signal is not always seen. The transition from even-electron to odd-electron ions is evidently considered to be forbidden.

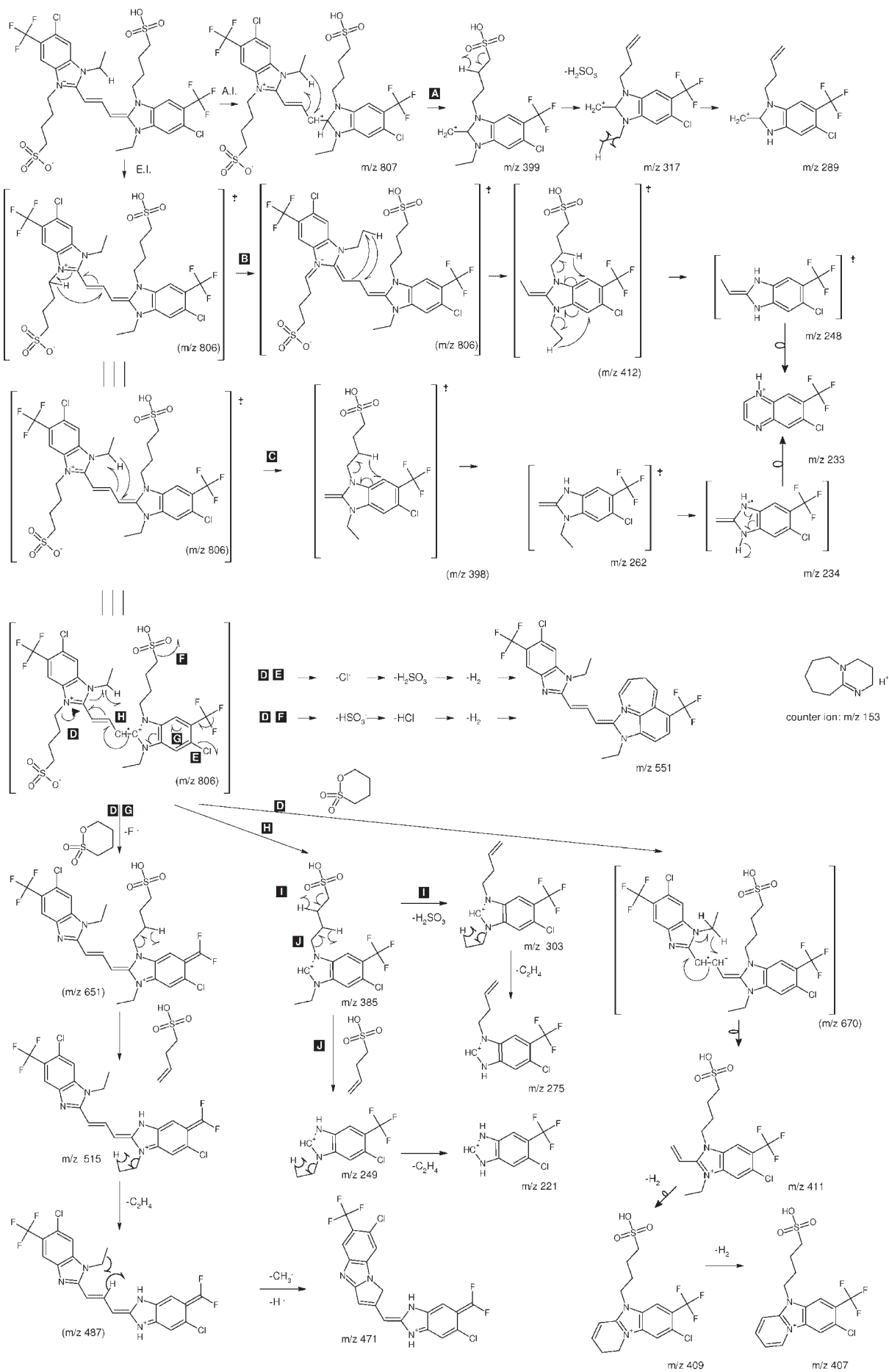
Within the framework of these assumptions, structural assignment of the major ions in the mass spectrum of compound I is relatively straightforward. Since a mass accuracy within 100 ppm leaves many possibilities for each ion, it is essential to use common MS knowledge to elaborate plausible ion structures and rationalise possible pathways, although they are not all proven in specific  $\text{MS}^n$  experiments. Scheme 1 starts from the intact release of the zwitterionic structure and subsequent ionisation in the seldedge by either EI leading to  $\text{M}^{+\bullet}$  ( $m/z$  806, not seen) or by AI involving the uptake of a  $\text{H}^+$  or  $\text{K}^+$  to result in the ions at  $m/z$  807 and 845, respectively. [Ions with  $m/z$  values in parentheses are not detected but drawn to clarify the fragmentation scheme.] The majority of the fragmentation evidently starts from the  $\text{M}^{+\bullet}$ , undergoing the well-known cleavages and rearrangements from gas-phase MS. Note the detection of the radical daughter ions at  $m/z$  262, 248 and 234, whose formation from even-electron precursors such as adduct ions is to be excluded. Cleavage D might need additional clarification. A zwitterion can undergo EI: the  $\text{M}^{+\bullet}$  then loses the side chain on the quaternised N as a result of a common heterolytic cleavage. This leads to the elimination of the anionic side chain as a neutral and brings the quaternised ring nitrogen to a neutral state. After this fragmentation, the resulting structure stabilises by expelling a radical such as  $\text{Cl}^\bullet$ ,  $\text{F}^\bullet$  or  $\text{SO}_3\text{H}^\bullet$ , as indicated in pathways DE, DF, and DG, respectively. The absence of the likely intermediate fragment ions leaves schemes DE or DF as possible routes for formation of the ions at  $m/z$  551. The rest of the detected daughter ions are readily rationalised, except those at  $m/z$  399, 317 and 289. The former formally correspond to the fragment ions at  $m/z$  385 with an additional  $\text{CH}_2$  group. Looking at the various fragmentation schemes and multiple rearrangements, it is virtually impossible to conceive a logical pathway from the  $\text{M}^{+\bullet}$  ion. In contrast, fragmentation of the protonated molecules from AI provide an elegant route to all these daughter ions.

These assignments show that a substantial fraction of the TIC is indeed carried by radical ions, necessarily generated from  $\text{M}^{+\bullet}$ . Otherwise stated, the pathways are relevant to link experimental evidence with the relative contribution of AI and EI, a key aspect in the DI model as it is linked to the local energy regime at the surface.<sup>22–25</sup>

Figure 4 shows the negative ion mass spectra of compound I recorded with the same projectiles as used for the positive ions. Again  $\text{Ga}^+$  bombardment results in the major part of the TIC being associated with the low  $m/z$  atomic ions such as  $\text{H}^{\bullet-}$ ,  $\text{F}^-$  and  $\text{Cl}^-$ . Even the signal for the low mass structural ion  $\text{SO}_3^-$  at  $m/z$  80 has a rather disappointing intensity, barely above the practical threshold of 1000 counts for a P.I. dose of about  $10^{12}$ .<sup>28</sup> Detection of characteristic fragment ions at higher  $m/z$  values requires heavier monoatomic projectiles such as  $\text{Bi}^+$ , yielding a significant contribution of the ions between  $m/z$  100 and 400. Use of polyatomic projectiles intensifies this trend to an extent depending on the projectile. Specifically, application of  $\text{Bi}_5^{2+}$

**Table 4.** Theoretical mass, experimental mass, formula and mass accuracy (absolute value in ppm, from spectra with  $\text{Bi}_5^{2+}$  P.I.s) for positive ions from compound I

Experimental	Theory	Formula	ppm
220,994	221,009	$\text{C}_8\text{H}_5\text{ClF}_3\text{N}_2$	68
232,992	233,009	$\text{C}_9\text{H}_5\text{ClF}_3\text{N}_2$	73
234,001	234,017	$\text{C}_9\text{H}_6\text{ClF}_3\text{N}_2$	69
248,022	248,033	$\text{C}_{10}\text{H}_8\text{ClF}_3\text{N}_2$	46
249,019	249,041	$\text{C}_{10}\text{H}_9\text{ClF}_3\text{N}_2$	85
262,039	262,049	$\text{C}_{11}\text{H}_{10}\text{ClF}_3\text{N}_2$	37
275,047	275,056	$\text{C}_{12}\text{H}_{11}\text{ClF}_3\text{N}_2$	37
289,064	289,071	$\text{C}_{13}\text{H}_{13}\text{ClF}_3\text{N}_2$	27
303,082	303,088	$\text{C}_{14}\text{H}_{15}\text{ClF}_3\text{N}_2$	18
317,098	317,103	$\text{C}_{15}\text{H}_{17}\text{ClF}_3\text{N}_2$	16
385,057	385,060	$\text{C}_{14}\text{H}_{17}\text{ClF}_3\text{N}_2\text{O}_3\text{S}$	10
399,072	399,075	$\text{C}_{15}\text{H}_{19}\text{ClF}_3\text{N}_2\text{O}_3\text{S}$	9
407,056	407,044	$\text{C}_{16}\text{H}_{15}\text{ClF}_3\text{N}_2\text{O}_3\text{S}$	30
409,053	409,060	$\text{C}_{16}\text{H}_{17}\text{ClF}_3\text{N}_2\text{O}_3\text{S}$	18
411,072	411,076	$\text{C}_{16}\text{H}_{19}\text{ClF}_3\text{N}_2\text{O}_3\text{S}$	10
471,059	471,020	$\text{C}_{20}\text{H}_{10}\text{Cl}_2\text{F}_5\text{N}_4$	83
515,045	515,082	$\text{C}_{23}\text{H}_{18}\text{Cl}_2\text{F}_5\text{N}_4$	72
551,214	551,143	$\text{C}_{27}\text{H}_{22}\text{ClF}_6\text{N}_4$	129
807,153	807,127	$\text{C}_{31}\text{H}_{35}\text{Cl}_2\text{F}_6\text{N}_4\text{O}_6\text{S}_2$	33



**Scheme 1.** Structural assignment and tentative fragmentation routes for positive ions from I.

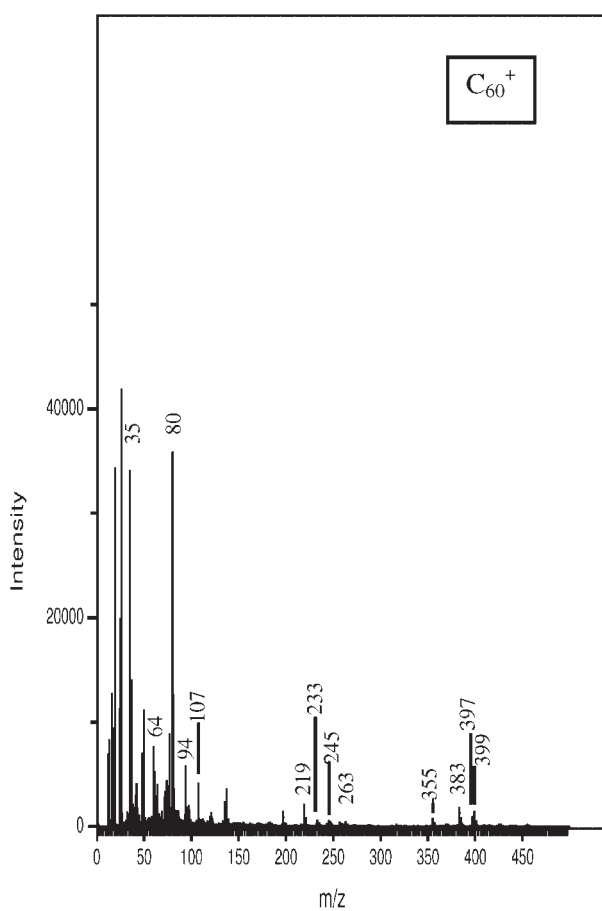
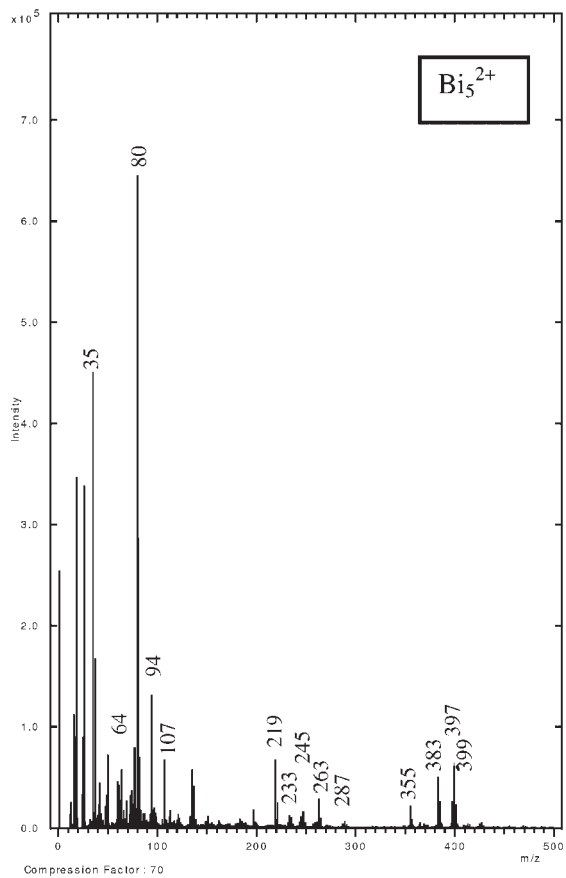
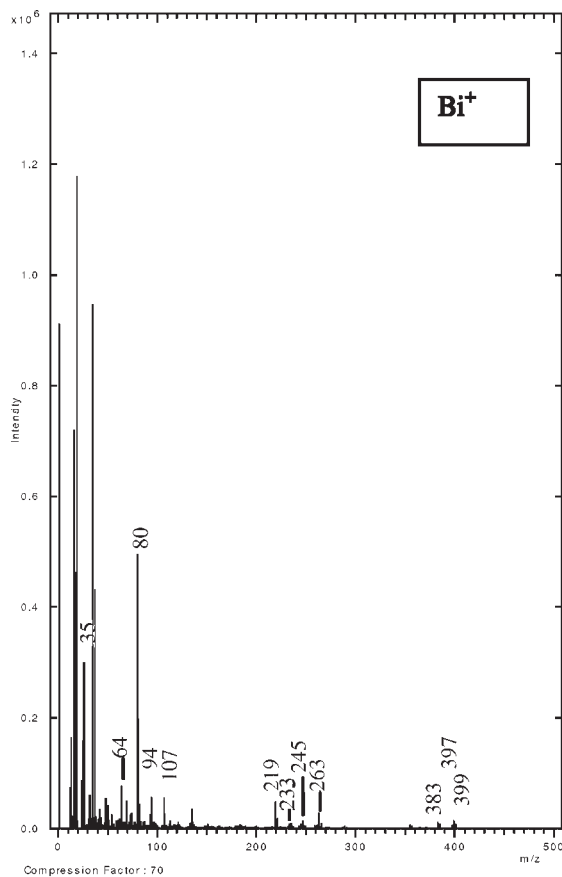
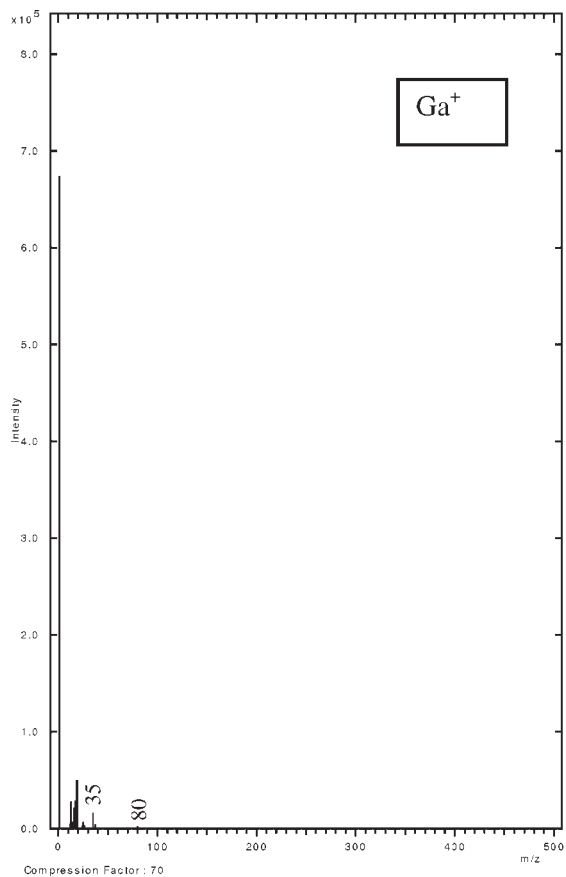
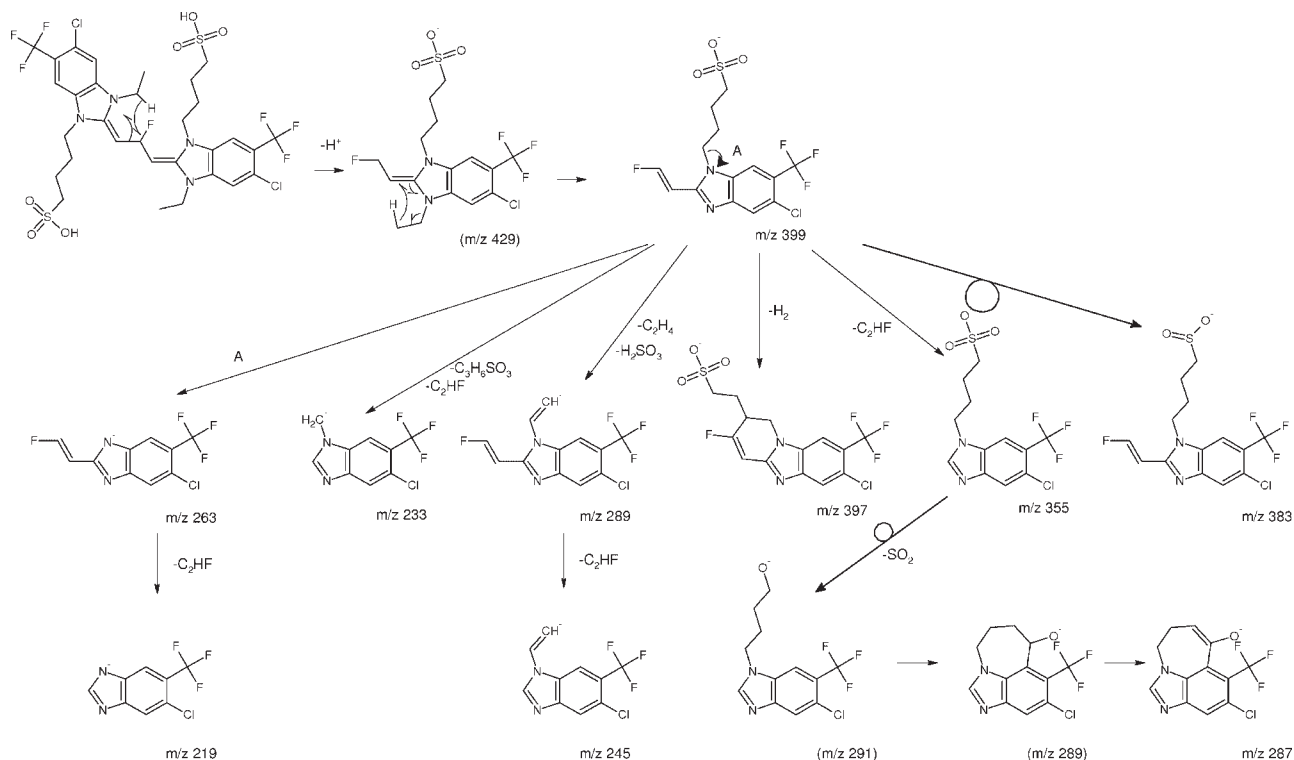


Figure 4. Negative ion mass spectra from I recorded with Ga<sup>+</sup>, Bi<sup>+</sup>, Bi<sub>5</sub><sup>2+</sup> and C<sub>60</sub><sup>+</sup> P.I.s.



**Scheme 2.** Proposed structures and tentative fragmentation routes for negative ions from I.

bombardment results in the mass spectrum with the most intense high  $m/z$  fragment ions. Apart from minor differences in the relative intensities,  $\text{Bi}_3^{2+}$  bombardment yields a mass spectrum closely resembling that obtained under  $\text{Bi}_5^{2+}$  conditions. The use of  $\text{SF}_5^+$  or  $\text{C}_{60}^+$  gives mass spectra with a lower relative abundance of the ions between  $m/z$  100 and 200 relative to the low  $m/z$  ions. The main difference between mass spectra taken with  $\text{C}_{60}^+$  and  $\text{SF}_5^+$  is that the base peaks are due to the  $\text{H}^-$  and  $\text{SO}_3^-$  ions, respectively.

Scheme 2 was elaborated using the exact mass measurements from Table 5 to assess the improvement of the polyatomic P.I. bombardment for diagnostic analysis of the analyte. From the data in Table 2 and the general observation that the experimentally measured  $m/z$  value must corre-

**Table 5.** Accurate mass determinations compared with theoretical mass yielding mass accuracy (absolute value in ppm, from spectra with  $\text{Bi}_5^{2+}$  P.I.s) for negative ions from compound I

Experimental	Theory	Formula	ppm
34,969	34,969	Cl	0
63,960	63,962	$\text{SO}_2$	31
79,956	79,957	$\text{SO}_3$	6
93,970	93,973	$\text{CH}_2\text{O}_3\text{S}$	27
106,978	106,981	$\text{C}_2\text{H}_3\text{O}_3\text{S}$	27
218,984	218,994	$\text{C}_8\text{H}_3\text{ClF}_3\text{N}_2$	56
232,999	233,010	$\text{C}_9\text{H}_5\text{ClF}_3\text{N}_2$	48
244,996	245,010	$\text{C}_{10}\text{H}_5\text{ClF}_4\text{N}_2$	57
263,001	263,001	$\text{C}_{10}\text{H}_4\text{ClF}_4\text{N}_2$	1
286,995	287,020	$\text{C}_{12}\text{H}_7\text{ClF}_3\text{N}_2\text{O}$	89
355,004	355,013	$\text{C}_{12}\text{H}_{11}\text{ClF}_3\text{N}_2\text{O}_3\text{S}$	24
383,035	383,044	$\text{C}_{14}\text{H}_{15}\text{ClF}_3\text{N}_2\text{O}_3\text{S}$	27
397,057	397,060	$\text{C}_{15}\text{H}_{17}\text{ClF}_3\text{N}_2\text{O}_3\text{S}$	10
399,033	399,076	$\text{C}_{15}\text{H}_{19}\text{ClF}_3\text{N}_2\text{O}_3\text{S}$	110

spond to within 50–100 ppm with the theoretical values, it is evident that most fragment ions must contain four F atoms. The only possibility for this seems to be ionisation through initial uptake of an  $\text{F}^-$  into an adduct with sufficient internal energy to undergo substantial breakdown. Binding of the  $\text{F}^-$  on the carbon in the middle of the  $\text{C}_3$ -bridge and similar H rearrangements and cleavages as seen for the positive ions allows most of the detected fragment ions to be rationalised.

The survey of the positive ion mass spectra of II in Fig. 5 obtained with the different projectiles confirms the trends seen before. In all cases the base peak is due to the  $\text{Na}^+$  ion but the corresponding signal accounts for over 80% of the TIC when monoatomic  $\text{Ga}^+$  is used. Turning to  $\text{Bi}^+$ ,  $\text{C}_{60}^+$  or  $\text{SF}_5^+$  and then to the doubly charged  $\text{Bi}_n^{2+}$  projectiles gradually increase the relative contribution from the ions in the  $m/z$  range between 50 and 100. Only in the case of the  $\text{Bi}_5^{2+}$  does the diagnostically interesting ion at  $m/z$  350 obtain a reasonable intensity relative to the base peak at  $m/z$  23. The accurate mass measurements in Table 6 and the fragment ion assignment in Scheme 3 show that the set of intense signals at  $m/z$  63, 72, 88, 149, 165, 202, 275 and 291 are associated with inorganic ions, perfectly fitting the empirical rules for speciation previously elaborated.<sup>25</sup> Specifically, the ions at  $m/z$  149 and 165 correspond to cationised sodium sulphite and sulphate, respectively. The substantially higher intensity of the ion at  $m/z$  149 than of that at  $m/z$  165 reflects the original presence of a sulphonate functionality in the solid. Small signals at high  $m/z$  values arise from the expected formation of dimeric adducts. The generation of  $\text{Na}_2\text{O}$  neutrals, detected as  $\text{H}^+$  adducts, fits within the general behaviour of oxysalts.<sup>28</sup> The detection of  $\text{NaCN}$ -related ions is typical for organic analytes with azaheterocyclic groups and reflects pyrolytic destruction. More directly relevant for the diag-

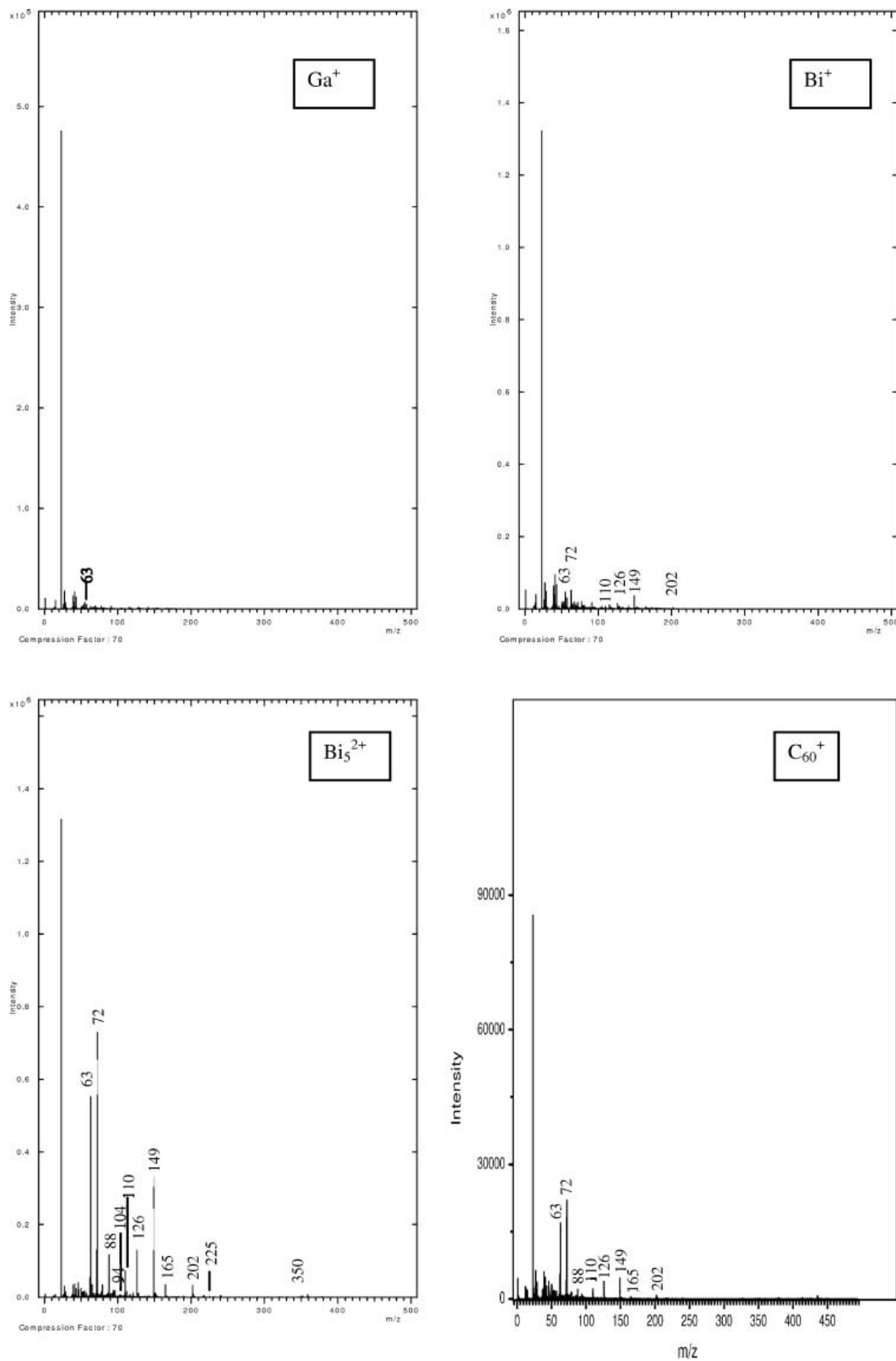
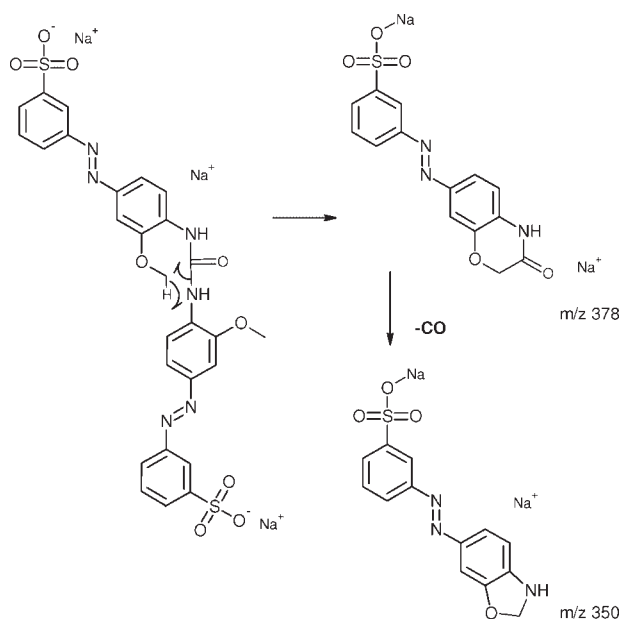


Figure 5. Positive ion mass spectra from compound II obtained with Ga<sup>+</sup>, Bi<sup>+</sup>, Bi<sub>5</sub><sup>2+</sup> and C<sub>60</sub><sup>+</sup> P.I.s.

**Table 6.** Positive ions from spectra obtained from II with theoretical mass and mass accuracy in ppm (from spectra with  $\text{Bi}_5^{2+}$  P.I.s). The majority of ions originate from Na cationisation of inorganic ions with only minor diagnostic value. Ions at  $m/z$  561, 661 and 677 are associated with Irganox 259 contamination

Experimental	Theory	Formula	ppm
62,983	62,982	$\text{Na}_2\text{OH}$	13
71,983	71,983	$\text{Na}_2\text{CN}$	6
87,978	87,978	$\text{Na}_2\text{CNO}$	6
93,946	93,947	$\text{Na}_2\text{SO}$	2
103,955	103,954	$\text{NaSO}_3\text{H}$	7
109,942	109,941	$\text{Na}_2\text{SO}_2$	4
125,937	125,936	$\text{Na}_2\text{SO}_3$	6
148,929	148,926	$\text{Na}_3\text{SO}_3$	17
164,924	164,921	$\text{Na}_3\text{SO}_4$	19
182,904	182,903	$\text{Na}_5\text{O}_6$	2
201,977	201,968	$\text{Na}_2\text{C}_6\text{H}_4\text{SO}_3$	44
202,985	202,976	$\text{Na}_2\text{C}_6\text{H}_5\text{SO}_3$	42
224,963	224,975	$\text{BiO}$	56
274,871	274,863	$(\text{Na}_2\text{SO}_3)_2\text{Na}$	30
290,861	290,857	$\text{Na}_5\text{S}_2\text{O}_7$	13
350,011	350,018	$\text{C}_{13}\text{H}_{10}\text{N}_3\text{Na}_2\text{SO}_4$	19
378,039	378,013	$\text{C}_{14}\text{H}_{10}\text{N}_3\text{Na}_2\text{SO}_5$	67
561,357	561,370	$\text{C}_{36}\text{H}_{49}\text{O}_5$	24
661,464	661,444	$\text{C}_{40}\text{H}_{62}\text{O}_6\text{Na}$	30
677,458	677,418	$\text{C}_{40}\text{H}_{62}\text{O}_6\text{K}$	60

nostic analysis of II are the high  $m/z$  signals from organic fragments. Specifically, the ions at  $m/z$  378 and 350 can be explained by the six-centered rearrangement of an amido group in the  $\text{Na}^+$ -cationised salt, followed by the expulsion of CO. The remaining signals at high  $m/z$  can be linked to the presence of commonly encountered UV-stabilisers. Specifically, the ion at  $m/z$  413 with reasonable intensity can be assigned to the fragmentation of  $\text{Na}^+$ -cationised Irganox 259



**Scheme 3.** Positive ion structures and tentative fragmentation routes for sodiated II.

(a phenolic antioxidant, used as a stabiliser for organic substrates, produced by Ciba Specialty Chemicals, Basel, Switzerland). Additionally, the  $\text{K}^+$  and  $\text{Na}^+$  adducts can be seen at  $m/z$  677 and 661, respectively.

The negative ion mass spectra of II, shown in Fig. 6, again contain only a few prominent peaks. Table 7 lists the accurate mass measurements of diagnostic anions of II and their tentative fragmentation routes are described in Scheme 4. Unlike with the positive ion mass spectra, the signal at  $m/z$  661 gives direct information about the MW in the form of the neutral minus a sodium cation. The lower  $m/z$  daughter ions are derived from initially released ion pairs undergoing electron capture ionisation. Fragmentation of the  $\text{M}^{\bullet-}$  reflects the generally observed tendency to form polycyclic fully aromatic ring systems to stabilise, in particular, the excess electron density of anions.<sup>29</sup> Intense signals at lower mass, i.e.  $m/z$  156, 171 and 182, must be associated with rather unusual ions in which the sulphonate functionality forms an additional ring to the aromatic group. The signals below  $m/z$  100 are readily associated with typical ions such as  $\text{SO}_3^-$  ( $m/z$  80),  $\text{CF}_2^-$  ( $m/z$  50),  $\text{CN}^-$  ( $m/z$  26), etc. The detection of the  $\text{CF}_2^-$  ions is a result of a memory effect from prior experiments with Krytox, a perfluorinated polyether produced by Du Pont (Wilmington, DE, USA).

### Quantitative evaluation of the ion intensities and diagnostic use of mass spectra

In the previous section the mass spectra taken with the different projectiles were compared with respect to the general appearance and the relative intensity of elemental and low  $m/z$  cluster ions relative to those of the high  $m/z$  structural ions. In general, the polyatomic  $\text{Bi}_3^{2+}$  and  $\text{Bi}_5^{2+}$  improved the structural specificity of mass spectra in that the relative contribution of the diagnostically most relevant ions to the TIC was increased compared with that of the low  $m/z$  signals. In order to investigate these effects more quantitatively, the ion intensity ratios of the most interesting ions were calculated. It is not feasible to discuss this large data matrix in detail and therefore Table 8 comprises a few illustrative figures to support the following observations:

- the positive ions from compound I allow the relative contribution of radical and even-electron fragment ions with about the same  $m/z$  values to be compared. The ratio of the sum of the intensities of radical ions at  $m/z$  248 and 262 over that for the even-electron ions at  $m/z$  249 and 303 shows that  $\text{Ga}^+$  projectiles apparently disfavour the formation of radicals. Although the ratio differences are rather small for the other projectiles, use of  $\text{SF}_5^+$  or  $\text{C}_{60}^+$  seems the most beneficial to detect specific structural information carried by radical fragments. This enhancement with  $\text{C}_{60}^+$  in comparison with  $\text{Ga}^+$  has already been described for Irganox 1010.<sup>30</sup>
- the ratio of low  $m/z$  fragment ions over those at high  $m/z$  (i.e.  $I_{249+248}/I_{303+385}$ ) shows that  $\text{Bi}_3^{2+}$  and  $\text{Bi}_5^{2+}$  bombardment leads to the highest relative intensities of the higher  $m/z$  fragment ions to the lower  $m/z$  ions. Inversely,  $\text{Ga}^+$  projectiles represent the other 'extreme' situation: fragmentation into lower  $m/z$  fragment ions seems to be stimulated;

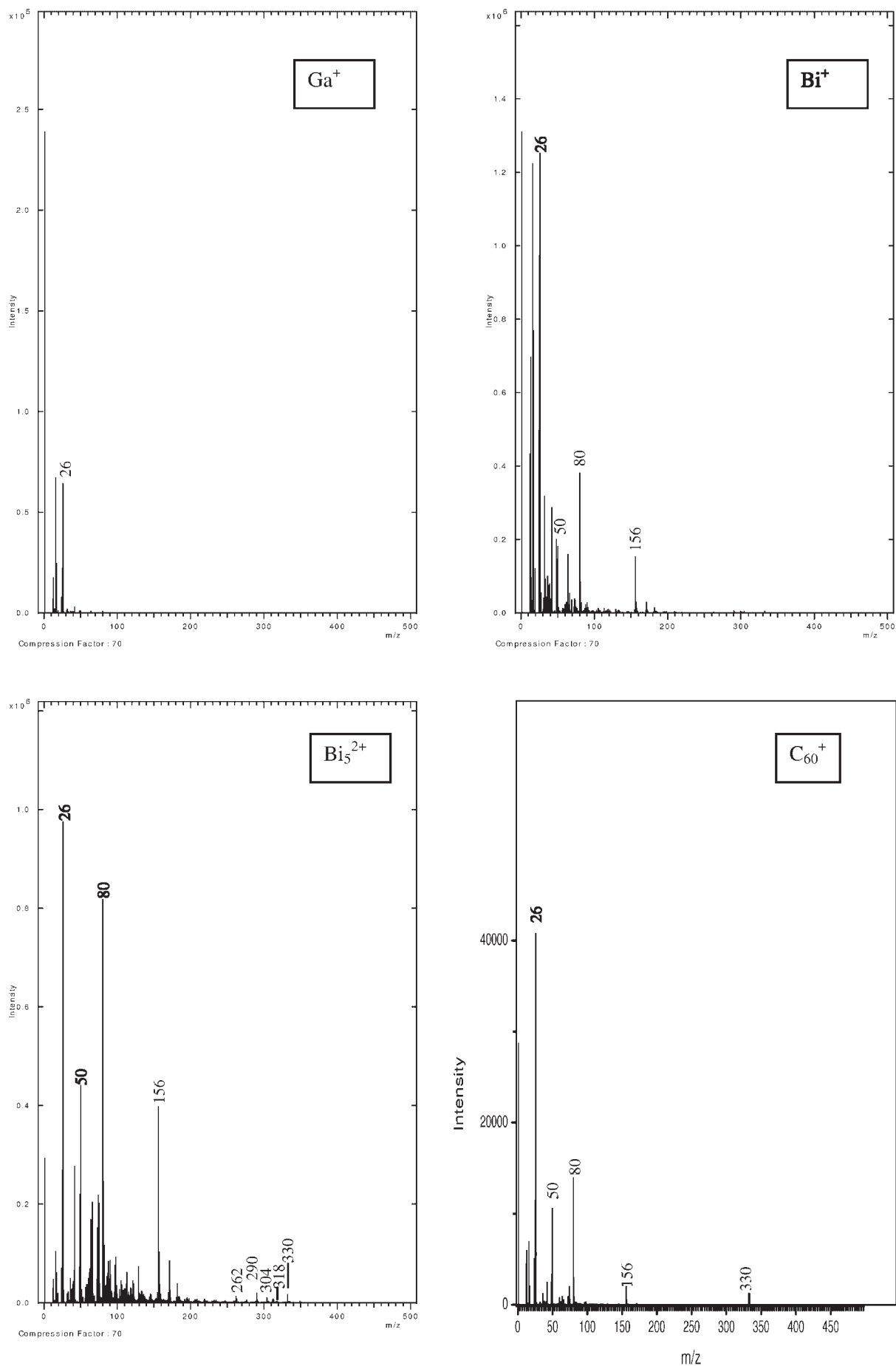
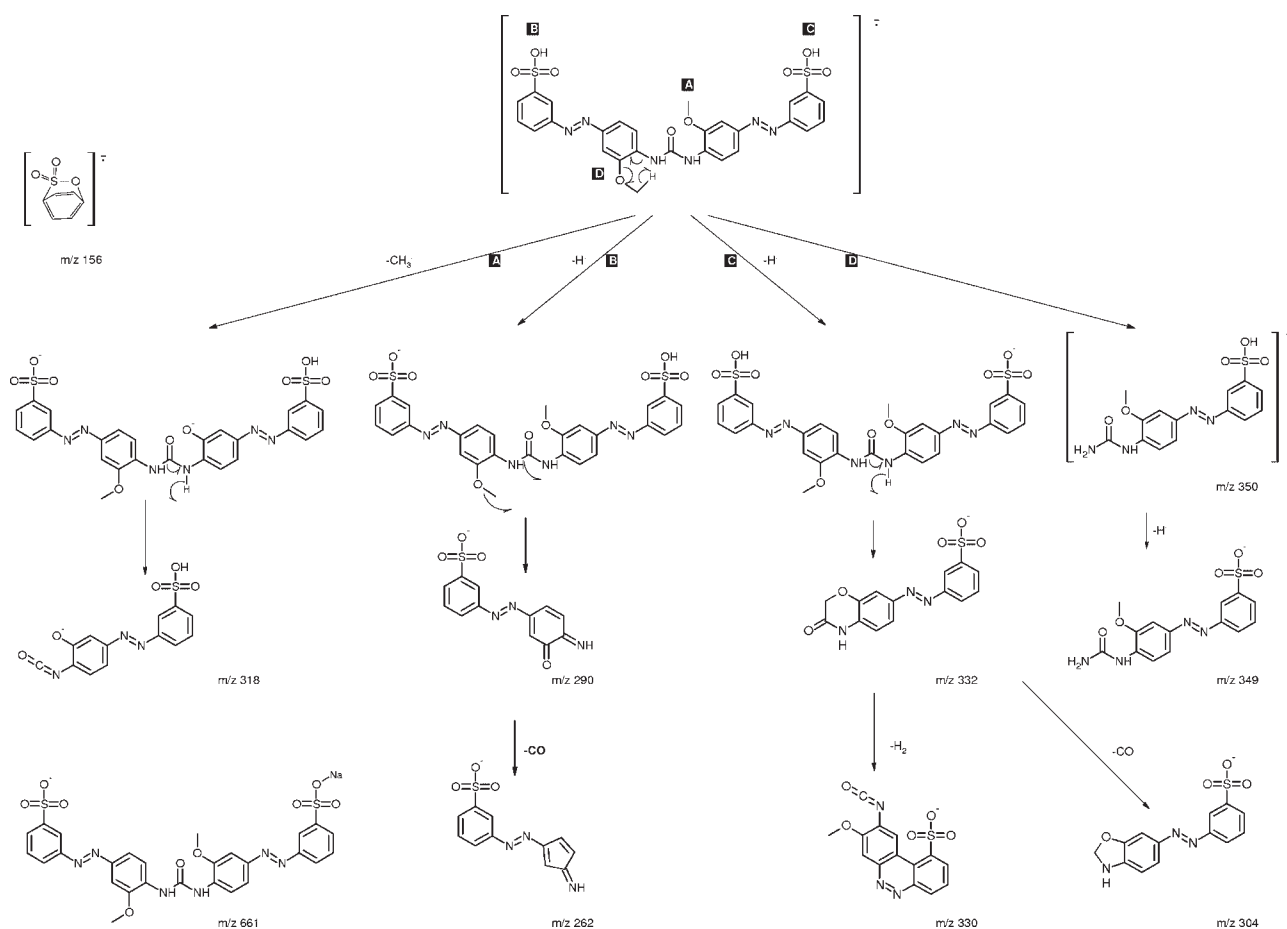


Figure 6. Negative ion mass spectra recorded from compound II using Ga<sup>+</sup>, Bi<sup>+</sup>, Bi<sub>5</sub><sup>2+</sup> and C<sub>60</sub><sup>+</sup> P.I.s.

**Table 7.** Theoretical and empirical  $m/z$  value and resulting mass accuracy (in ppm, from spectra with  $\text{Bi}_5^{2+}$  P.I.s) for diagnostic negative ions from II

Spectrum	Theory	Compound	ppm
26,004	26,003	CN	35
50,004	50,004	CF <sub>2</sub>	0
79,957	79,957	SO <sub>3</sub>	1
155,987	155,988	C <sub>6</sub> H <sub>4</sub> SO <sub>3</sub>	4
262,008	262,029	C <sub>11</sub> H <sub>8</sub> N <sub>3</sub> SO <sub>3</sub>	82
290,017	290,024	C <sub>12</sub> H <sub>8</sub> N <sub>3</sub> SO <sub>4</sub>	24
304,024	304,040	C <sub>13</sub> H <sub>10</sub> N <sub>3</sub> SO <sub>4</sub>	53
318,017	318,019	C <sub>13</sub> H <sub>8</sub> N <sub>3</sub> SO <sub>5</sub>	6
330,009	330,019	C <sub>14</sub> H <sub>8</sub> N <sub>3</sub> SO <sub>5</sub>	29
332,033	332,035	C <sub>14</sub> H <sub>10</sub> N <sub>3</sub> SO <sub>5</sub>	5
661,083	661,079	C <sub>27</sub> H <sub>22</sub> N <sub>6</sub> S <sub>2</sub> O <sub>9</sub> Na	6

- for negative ions from I,  $\text{Ga}^+$  impact fails to generate detectable organic fragments at high  $m/z$  which hampers the comparison of the data to some extent. Nevertheless, it is clear that the monoatomic P.I. guns excel in generating abundant signals from elemental ions and small inorganic cluster ions. The use of  $\text{Ga}^+$  leads to the complete disappearance of the structurally significant organic high  $m/z$  ions as opposed to the experiments with  $\text{Bi}^+$ . Comparing the different polyatomic projectiles, it appears that  $\text{C}_{60}^+$ ,  $\text{Bi}_3^{2+}$  and  $\text{Bi}_5^{2+}$  are almost equivalent and only slightly better than  $\text{SF}_5^+$ ;
- compound II is a good example to provide evidence of how the type of P.I. source affects the balance between the generation of organic structural ions at high  $m/z$  and that of the inorganic small (cluster) ions for a given analyte with

**Scheme 4.** Tentative fragmentation and structural assignment for negative ions from II.**Table 8.** Selected relative ion signal intensities from compounds I and II for negative and positive ions from spectra obtained with different P.I. guns

Compound	Polarity	Ions ( $m/z$ )	$\text{Bi}_5^{2+}$	$\text{Bi}_3^{2+}$	$\text{Bi}^+$	$\text{SF}_5^+$	$\text{Ga}^+$	$\text{C}_{60}^+$
I	+	248+262/249+303	0.83	0.84	0.92	0.97	0.68	1.07
		248+249/385+303	0.46	0.50	0.77	0.74	0.97	0.80
	–	35+64+80/219+263	20	20	35	22	n/a	17
		35+64+80/355+383+399	11	17	50	31	n/a	10
II	+	350+378/149+165	0.012	0.010	0.014	0.009	0	0.031
		149/165	10	10	7	10	6	9
	–	262+290+332/26	0.037	0.054	0.005	0.023	0	0.0031
		262+290+332/26+80	0.020	0.026	0.004	0.013	0	0.0019

sulphonate functionalities. Again,  $\text{Ga}^+$  does not yield information on the organic structure from the positive ion peaks seen. All the other projectiles perform better, with  $\text{C}_{60}^+$  showing the highest ratio. However, the number of counts in the different peaks must also be considered. The absolute intensities of all peaks considered here are a factor 10 higher for  $\text{Bi}_n^{2+}$  bombardment than for  $\text{Bi}^+$  projectiles. The organic signals ( $m/z$  350 and 378) have similar intensities in the  $\text{Bi}_n^{2+}$  and  $\text{C}_{60}^+$  spectra while the inorganic signals ( $m/z$  149 and 165) are a factor of 3 higher for  $\text{Bi}_n^{2+}$  than for  $\text{C}_{60}^+$  projectiles. As a result, the ratio of organic over inorganic ions becomes lower for  $\text{Bi}_n^{2+}$  but that is because the sulphonate peaks have higher intensity than in the case of  $\text{C}_{60}^+$  while the organic ions have similar intensity;

- as stated previously,<sup>28</sup> the intensity ratio of the positive ions  $m/z$  149 and 165 from compound II can be used to assess the relative importance of the direct emission versus oxido-reductive selvedge processes. Interestingly, the use of polyatomic P.I.s, either  $\text{Bi}_n^{2+}$ ,  $\text{SF}_5^+$  or  $\text{C}_{60}^+$ , gives rise to a pronounced contribution from the cationised sulphite ions, better reflecting the original stoichiometry than the sodium sulphate adducts at  $m/z$  165. This observation points to a better specificity of the polyatomic guns in terms of inorganic speciation;
- the ratios for the negative ions from compound II essentially confirm the previous results:  $\text{Ga}^+$  bombardment does not allow the high  $m/z$  organic fragment ions to be detected, in contrast to the heavier  $\text{Bi}^+$  monoatomic projectile. However, incorporation of more atoms in the impinging particle apparently leads to more interesting conditions to generate structural ions relative to the low  $m/z$  inorganic clusters and this is in particular the case for  $\text{Bi}_n^{2+}$ .

## CONCLUSIONS

A recent reviewer discussing the progress in ion gun development for S-SIMS quoted Benninghoven who stated that the molecular SIMS community, ‘has probably for long been shooting with the wrong bullets’.<sup>3</sup> The results discussed in this paper indeed support this vision in that  $\text{Ga}^+$  ions perform worse than monoatomic  $\text{Bi}^+$  and both of them are certainly inferior to the polyatomic projectiles in producing mass spectra with high ion counts per peak and high diagnostic value. This means that the relative importance of the high  $m/z$  ions increases in comparison with atomic ions and the less structurally specific cluster ions. Even within the set of organic fragments, there is a clear tendency to reduce the contribution of the lower  $m/z$  daughter ions, often resulting from complex skeletal rearrangements and thereby presenting less diagnostic value, relative to the high  $m/z$  ions, resulting from the initial loss of rather small radicals or neutrals. This trend is also clear in this study, even though the compounds have highly conjugated backbones that favour formation of aromatic rings.

The observations made with respect to the general features of the mass spectra taken with different mono- and polyatomic projectiles can readily be linked to the current state of knowledge on cluster sputtering. Several publications, mainly based on molecular dynamics studies, point to the same general features of the enhanced desorption

when using cluster projectiles for the sputtering of organic solids.<sup>3,15,31–36</sup> It is shown that the enhanced desorption (subsequently yielding a higher probability for ionisation and thus enhanced ion yield) is linked to the larger energy density which is deposited in the top surface region when using big clusters (the focus in the literature is particularly on  $\text{C}_{60}^+$ ) in comparison with metallic projectiles.<sup>3,15</sup> The highest ejection yields are associated with clusters that deposit their incident energy 15–20 Å below the surface and that are built up of atoms with a mass close to the masses of the target atoms’ masses.<sup>31–33</sup> Specifically due to the good mass match, a  $\text{C}_{60}^+$  ion can split apart upon impact on organic materials sending C atoms in all directions, depositing their energy in a spherical region and exciting the near-surface region of the sample. This causes crater formation and the material of interest is ejected in a mesoscopic process, yielding a collective outward molecular motion.<sup>34,35</sup> The processes occurring upon bombardment with LMIG metal clusters such as  $\text{Au}_n^+$  or  $\text{Bi}_n^{q+}$  are less studied. They are believed also to yield improved desorption, rather than ionisation, but probably in a different way from  $\text{C}_{60}^+$ . The mass match is not as good as with  $\text{C}_{60}^+$  projectiles and based on P.I. structures these yield enhancements seem not to be related to an increased deposited energy density. The ion yield enhancement is suggested by Nagy and Walker to arise from multiple, concerted particle impacts on the sample.<sup>37</sup>

While the general qualitative interpretation of the mass spectra is rather simple, the more sophisticated quantitative assessment of specific ion intensity ratios does not yet produce a clear picture about the change in internal energy distribution and the distribution between even-electron and radical precursor ion formation. Clearly developments in ion guns are proceeding faster than a detailed understanding as to why the newer projectiles effectively perform better. Our data further confirm that polyatomic P.I.s will improve the potential of S-SIMS. There is in general a substantial increase in the ion yield by a factor of at least 10 for the diagnostic and analytically most important ions, specifically those at high  $m/z$ . This improvement in detection capabilities is noteworthy especially because the introduction and maturing of the TOF technology has pushed S-SIMS instrumentation almost to its physical limits in terms of transmission, detector efficiency and duty cycle factor. In addition, an improved balance between high and low  $m/z$  ions is especially required to obtain the molecular adduct ions (e.g. anion at  $m/z$  661 and cations at  $m/z$  350 and 378 from II, all structural fragment ions from compound I in the negative ion mode) or to detect minor contaminants at extremely low concentrations such as e.g. UV stabilisers (Irganox 259) from plastics.

## Acknowledgements

RDM is indebted to the Institute for the Promotion of Innovation through Science and Technology in Flanders (IWT-Vlaanderen) for a Ph.D. grant. The research was funded by the the FWO Flanders. We would like to acknowledge that this research has been supported by the Nano-beams NoE, which was given a financial contribution by the European Commission. This paper only reflects the view of the authors.

## REFERENCES

1. De Mondt R, Van Vaeck L, Lenaerts J. *J. Am. Soc. Mass Spectrom.* 2007; **18**: 382. DOI: 10.1016/j.jasms.2006.09.029.
2. Delcorte A, Médard N, Bertrand P. *Anal. Chem.* 2002; **74**: 4955.
3. Wucher A. *Appl. Surf. Sci.* 2006; **252**: 6482.
4. Gillen G, Roberson S. *Rapid Commun. Mass Spectrom.* 1998; **19**: 1303.
5. Delcorte A, Poleunis C, Bertrand P. *Appl. Surf. Sci.* 2006; **252**: 6494.
6. Appelhans AD, Delmore JE. *Anal. Chem.* 1989; **61**: 1087.
7. Lenaerts J, Gijbels R, Van Vaeck L, Verlinden G, Geuens I. *Appl. Surf. Sci.* 2003; **203/204**: 614.
8. Kollmer F. *Appl. Surf. Sci.* 2004; **231**: 153.
9. Fletcher JS, Lockyer NP, Seetharaman V, Vickerman JC. *Anal. Chem.* 2007; **79**: 2199.
10. Jones EA, Lockyer NP, Vickerman JC. *Int. J. Mass Spectrom.* 2007; **260**: 146.
11. Kötter F, Benninghoven A. *Appl. Surf. Sci.* 1998; **133**: 47.
12. Hagenhoff B, Pfitzer K, Tallarek E, Kock R, Kersting R. *Appl. Surf. Sci.* 2004; **231/232**: 196.
13. Wong SCC, Hill R, Blenkinsopp P, Lockyer NP, Weibel DE, Vickerman JC. *Appl. Surf. Sci.* 2003; **203/204**: 219.
14. Zhua Z, Kelley MJ. *Appl. Surf. Sci.* 2006; **252**: 6619.
15. Delcorte A. *Phys. Chem. Chem. Phys.* 2005; **7**: 3395.
16. Solomko V, Verstraete M, Delcorte A, Garrison BJ, Gonze X, Bertrand P. *Appl. Surf. Sci.* 2006; **252**: 6459.
17. Lenaerts J, Van Vaeck L, Gijbels R, Van Luppen J. *Rapid Commun. Mass Spectrom.* 2004; **3**: 257.
18. Fuoco ER, Gillen G, Wijesundara MJB, Wallace WE, Hanley L. *J. Phys. Chem. B* 2001; **18**: 3950.
19. Postawa Z. *Appl. Surf. Sci.* 2004; **231**: 22.
20. Schueler BW. *Microsc. Microanal. Microstruct.* 1992; **3**: 119.
21. Weibel D, Wong S, Lockyer N, Blenkinsopp P, Hill R, Vickerman JC. *Anal. Chem.* 2003; **75**: 1754.
22. Van Vaeck L, Adriaens A, Gijbels R. *Mass Spectrom. Rev.* 1999; **18**: 1.
23. Van Vaeck L, Claereboudt J, De Waele J, Esmans E, Gijbels R. *Anal. Chem.* 1985; **57**: 2944.
24. Van Vaeck L, Struyf H, Van Roy W, Adams F. *Mass Spectrom. Rev.* 1994; **13**: 189.
25. Van Vaeck L. *Encyclopedia of Analytical Science*, (2nd edn), Worsfold P, Townshend A, Poole C (eds). Elsevier Ltd.: Oxford, 2004; 237.
26. Pachuta SJ, Cooks RG. *Chem. Rev.* 1987; **87**: 647.
27. Cooks RG, Busch KL. *Int. J. Mass Spectrom. Ion Processes* 1983; **53**: 111.
28. Van Ham R, Van Vaeck L, Adams FC, Adriaens A. *Anal. Chem.* 2004; **76**: 2609.
29. Van Vaeck L, Bennett J, Van Espen P, Schweikert E, Gijbels R, Adams F, Lauwers W. *Org. Mass Spectrom.* 1989; **24**: 797.
30. Delcorte A, Yunus S, Wehbe N, Nieuwjaer N, Poleunis C, Felten A, Houssiau L, Pireaux J-J, Bertrand P. *Anal. Chem.* 2007; **79**: 3673.
31. Russo MF, Jr, Szakal C, Kozole J, Winograd N, Garrison BJ. *Anal. Chem.* 2007; **79**: 4493.
32. Smiley EJ, Winograd N, Garrison BJ. *Anal. Chem.* 2007; **79**: 494.
33. Russo MF, Jr, Garrison BJ. *Anal. Chem.* 2006; **78**: 8317.
34. Delcorte A, Garrison BJ. *J. Phys. Chem. C* 2007; **111**: 15312.
35. Delcorte A, Garrison BJ. *Nucl Instr. Meth. Phys. Res. B* 2007; **255**: 223.
36. Webb R, Chatzipanagiotou A. *Nucl Instr. Meth. Phys. Res. B* 2006; **242**: 413.
37. Nagy G, Walker AV. *Int. J. Mass Spectrom.* 2007; **262**: 144.